Supplementary Information

Fast response/recovery and sub-ppm ammonia gas sensors based on a novel V_2CT_x@MoS_2 composite

Manyu Luo [a,b], Xingpeng Huang [a,b], Deshou Xiong [a,b], Sijin Cai[b] ,Shuang Li [b]* , Zhenhong Jia [a]* and Zhixian Gao[b]*

[a]School of Information Science and Engineering, Xinjiang University, Urumqi 830046, China
[b]Tianjin Key Laboratory of Risk Assessment and Control Technology for Environment and Food Safety, Tianjin Institute of Environment and Operational Medicine, Tianjin 300050, China
*Corresponding authors.
E-mail：
liza3320@163.com(Shuang Li)
jzhh@xju.edu.cn(Zhenhong Jia)
gaozhx@163.com(Zhixian Gao)

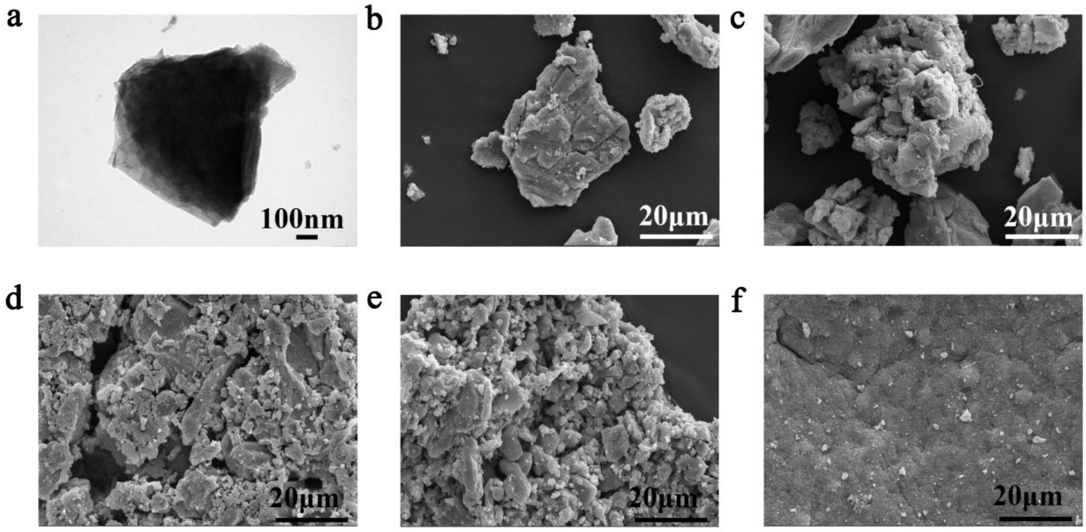

Fig. S1 Topography of synthetic materials. a) TEM image of V_2CT_x.b-f) SEM images of V_2CT_x@MoS_2 composite materials. b) V_2CT_x@MoS_2-0.5, c) V_2CT_x @MoS_2-0.75, d) V_2CT_x @MoS_2-1, e) V_2CT_x @MoS_2-2 and f) V_2CT_x @MoS_2- 4.

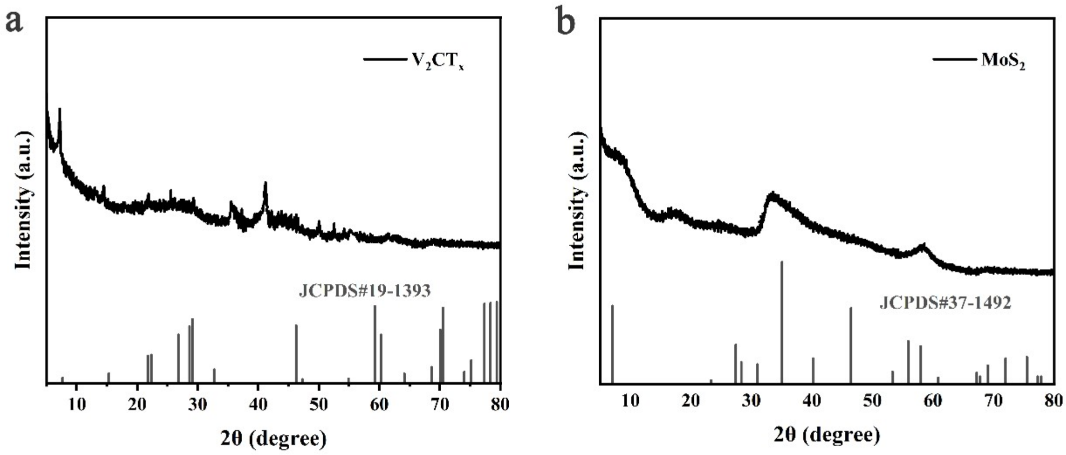

Fig. S2 Spectra of synthesized samples with labeled standard XRD cards. a) V_2CT_x, b) MoS_2.

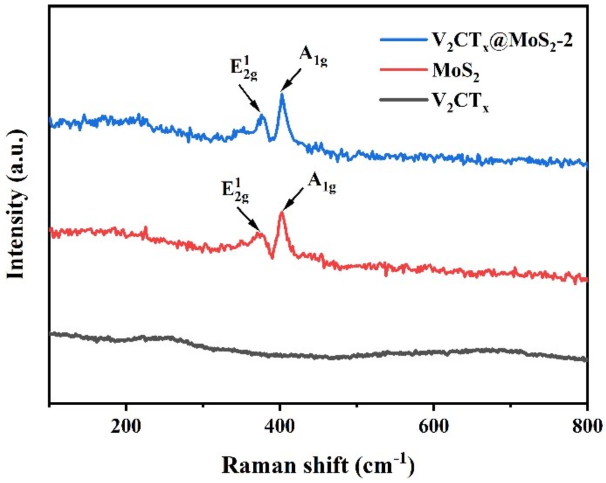

Fig. S3 Raman spectra of V_2CT_x, MoS_2, and V_2CT_x@MoS_2-2.

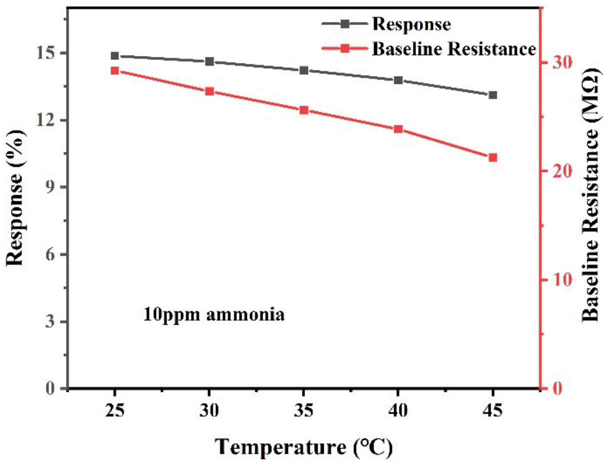

Fig. S4 Response and baseline resistance of V_2CT_x@MoS_2 based sensors to 10 ppm ammonia at different temperatures.

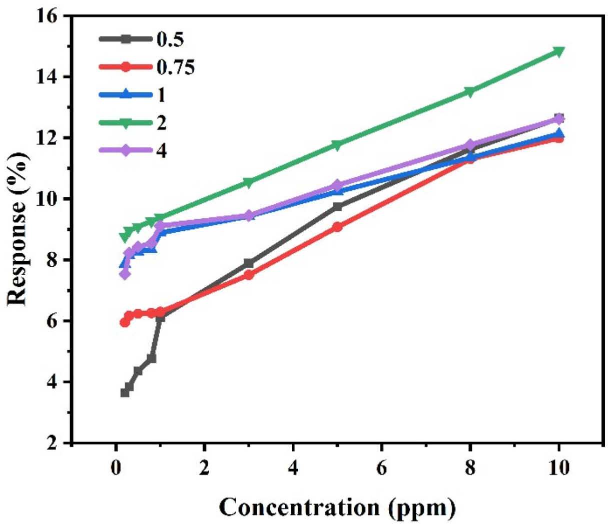

Fig. S5 Comparison line plot of the response of V_2CT_x @MoS_2 composites with different mass ratios in the range of ammonia concentrations from 0.2 to 1 ppm.

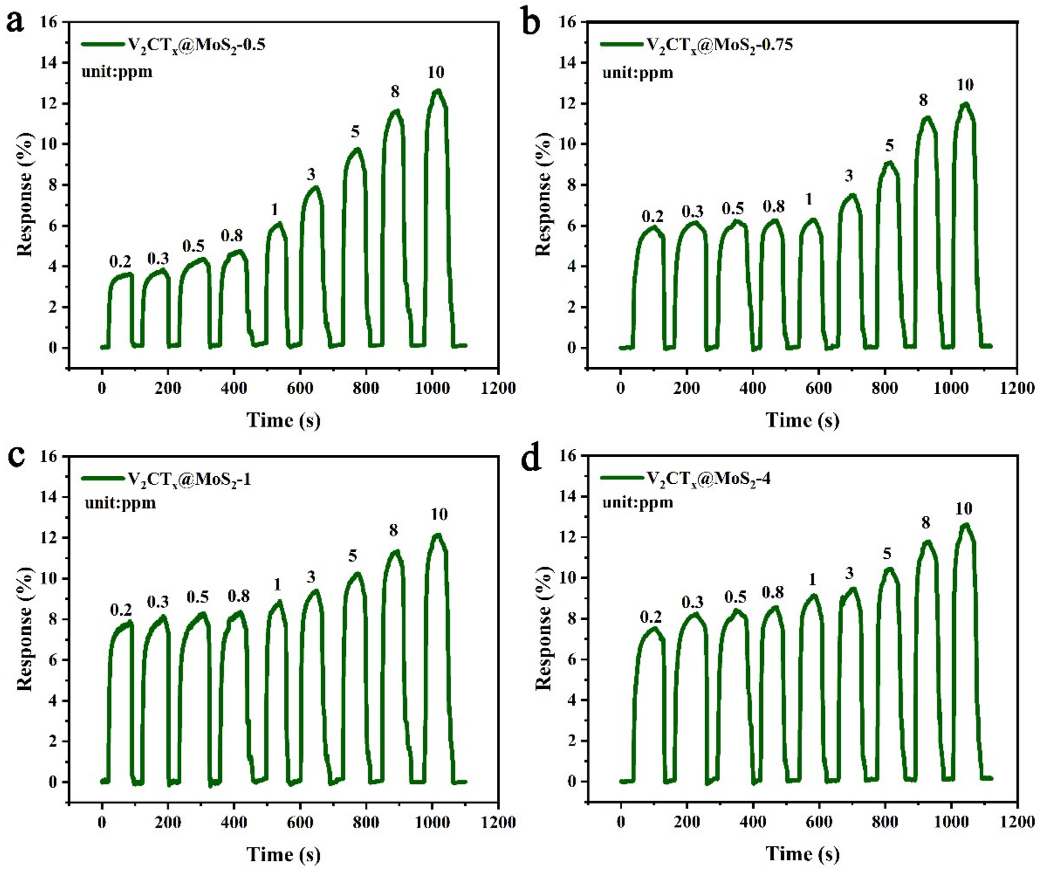

Fig. S6 Sensing performance test of V_2CT_x and MoS_2 composite sensors with different masses at room temperature within 0.2-10ppm concentration and at 43% relative humidity. a) V_2CT_x @MoS_2-0.5, b) V_2CT_x @MoS_2-0.75, c) V_2CT_x @MoS_2-1 and d) V_2CT_x @MoS_2- 4.

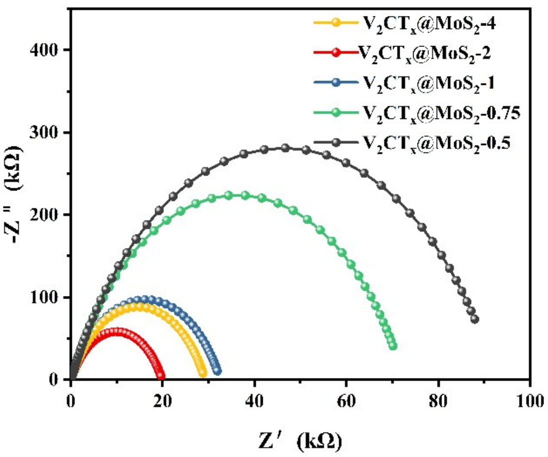

Fig. S7 Nyquist diagram of V_2CT_x and MoS_2 composites at different mass ratios.

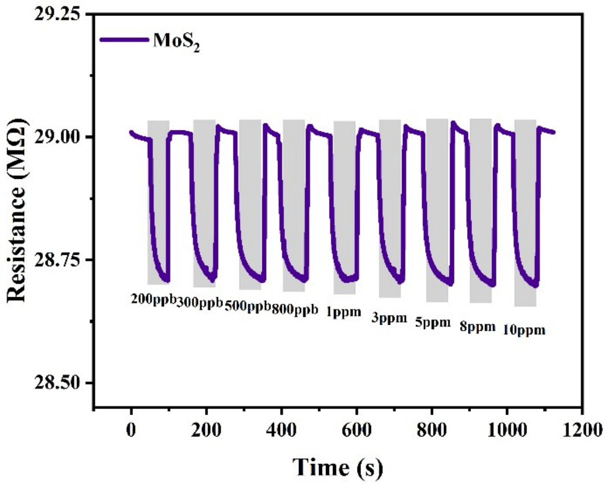

Fig. S8 Variation in resistance of a pure MoS_2 sensor at different ammonia concentrations at room temperature.

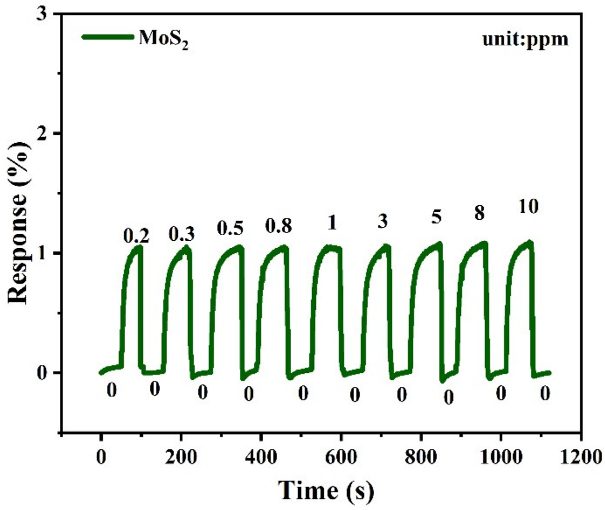

Fig. S9 Dynamic response of a pure MoS_2 sensor at different ammonia concentrations at room temperature.

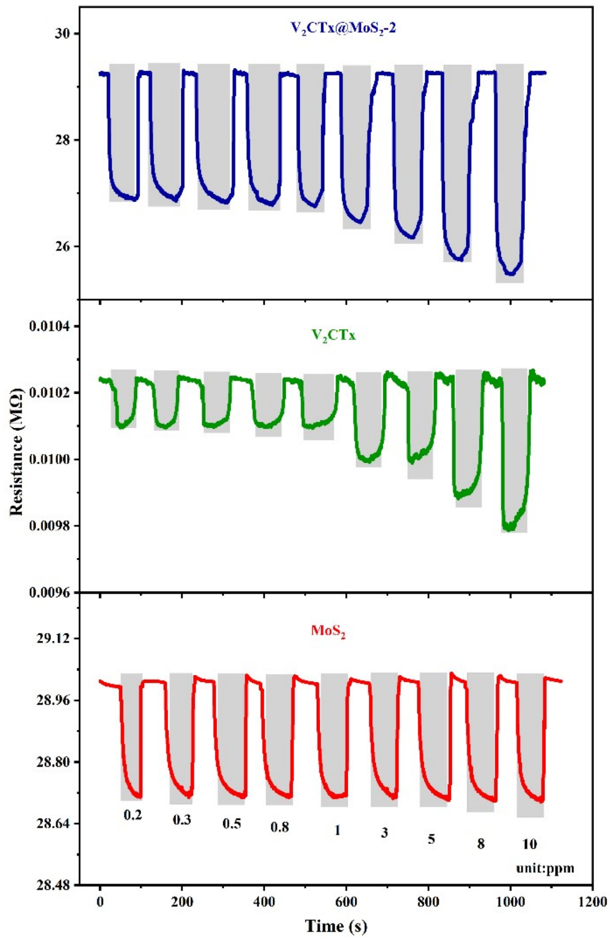

Fig. S10 Comparison of the resistance of pure MoS_2 sensor, pure V2CT$_x$ sensor and V_2CT_x@MoS_2-2 sensor with ammonia concentration.

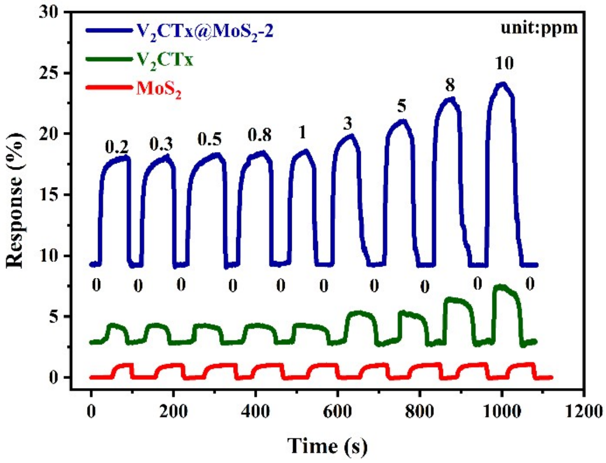

Fig. S11 Comparison of the responses of pure MoS_2 sensors, pure V_2CT_x sensors and V_2CT_x@MoS_2-2 sensors with ammonia concentration.

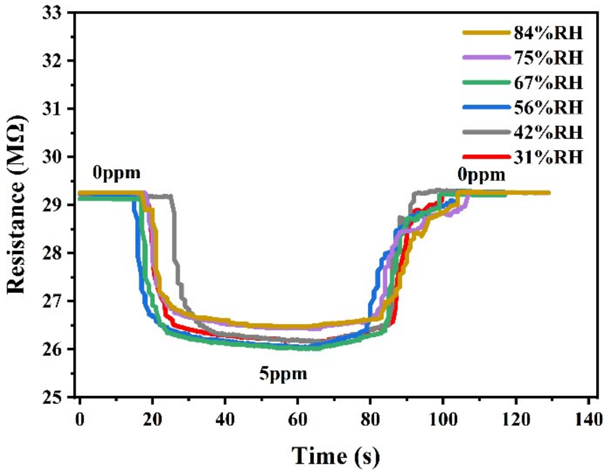

Fig. S12 Variation of resistance of V_2CT_x@MoS_2-2 composite sensor at room temperature under different humidity.

Computational details

Spin-polarized DFT calculations were performed using the Vienna *ab initio* simulation package (VASP) code[1, 2]. The projector augmented wave method (PAW) and the Perdew–Burke–Ernzerhof (PBE) exchange-correlation function were performed to describe both valence electron and core interactions [3, 4]. A plane wave basis with a kinetic cut-off energy of 450 eV was utilized. All structures were fully optimized until energy and residual force convergence criteria of 10^{-5} eV and 0.03 eV/Å were met. The DFT-D3 method[5] was utilized for accurate estimation of adsorption strength. Sampling was conducted using a 1 × 1 × 1 Monkhorst-Pack grid for general calculations, while a dense 3 × 3 × 1 Monkhorst-Pack grid was employed for electronic property calculations.

The difference in charge density is defined as $\Delta\rho = \rho_{*mol} - \rho_{*} - \rho_{mol}$, where ρ_{*mol}, ρ_{*}, and ρ_{mol} represent the electron densities of the slab with the adsorbed molecule (including NH_3, CH_2O, CH_3OH, and CH_3COCH_3), the isolated slab, and the isolated molecule, respectively. Additionally, the adsorption energy E_{ads} per molecule is defined as $E_{ads} = E_{*mol} - E_{*} - E_{mol}$, where E_{*mol} stands for the energy of the monolayer with the adsorbed molecule, E_{*} is the energy of a clear monolayer, and E_{mol} is the energy of an isolated molecule under vacuum.

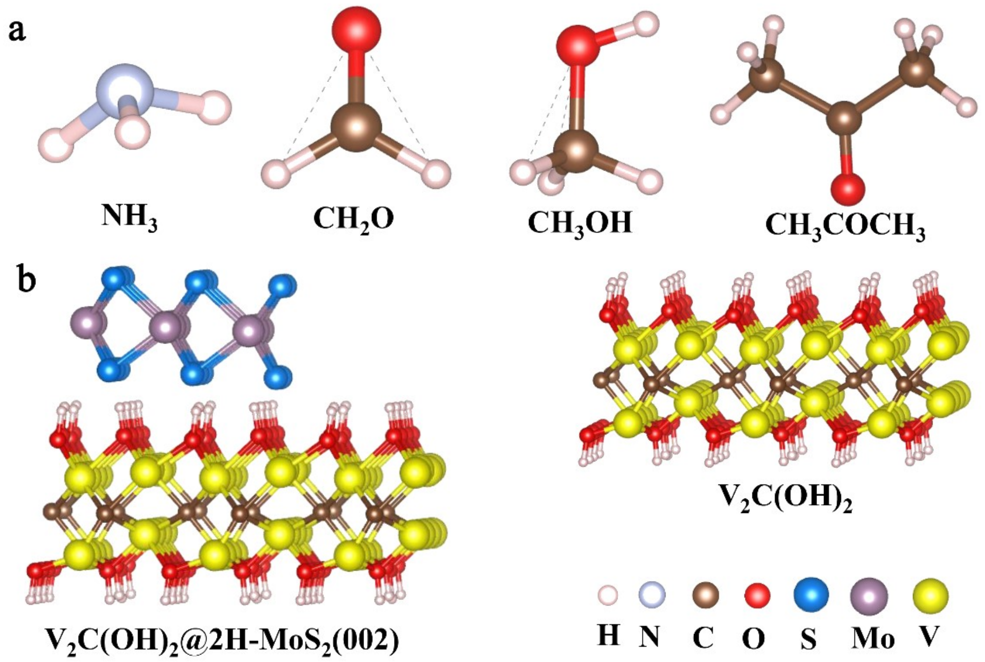

Fig.S13 a) The constructed initial models of ammonia (NH_3), acetone (C_3H_6O), methanol (CH_4O) and formaldehyde (CH_2O), b) $V_2C(OH)_2$ and $V_2C(OH)_2$@2H-MoS_2(002).

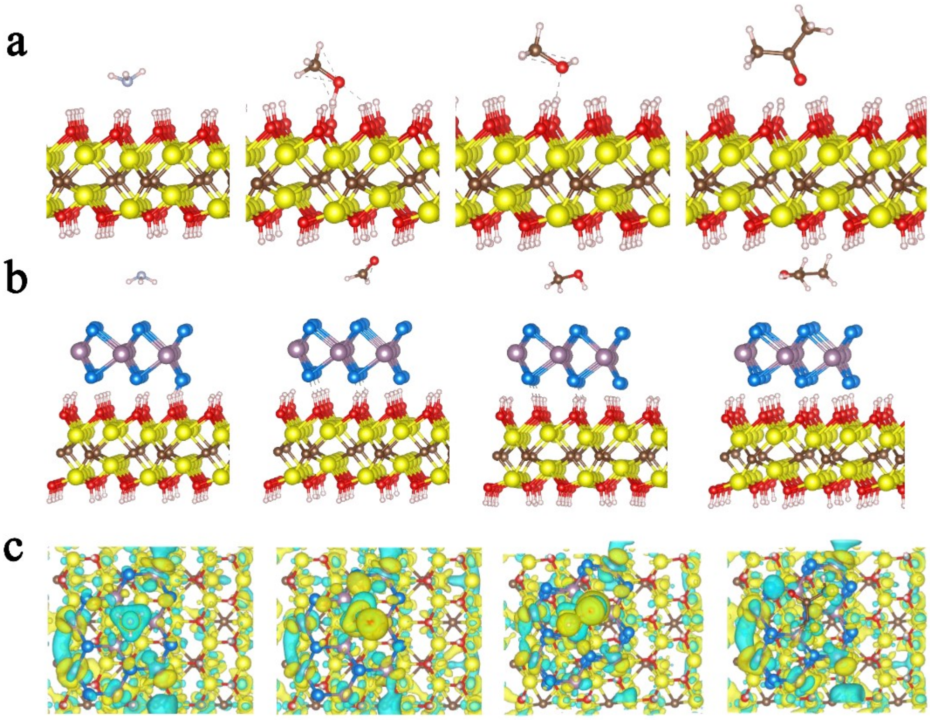

Fig.S14 Model diagram of a) $V_2C(OH)_2$ adsorbed ammonia (NH_3), acetone (C_3H_6O), methanol (CH_4O) and formaldehyde (CH_2O) molecules, b) $V_2C(OH)_2$@MoS_2 adsorbed ammonia (NH_3), acetone (C_3H_6O), methanol (CH_4O) and formaldehyde (CH_2O) molecules, c) Difference in charge density of $V_2C(OH)_2$@MoS_2 model with ammonia, acetone, methanol, and formaldehyde molecules.

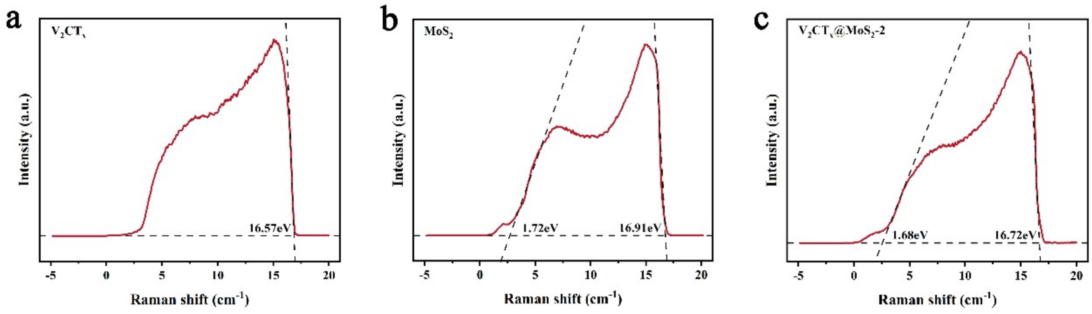

Fig.S15 UPS spectra of a) V_2CT_x, b) MoS_2, c) V_2CT_x@MoS_2-2.

Table S1. Comparison of the performance of the proposed sensor and previously reported ammonia sensors

Material	Detection range (ppm)	LOD (ppm)	Response time(s)	Recovery time(s)	Sensitivity	Ref.
Nb_2CT_x /PANI	1-100	1	105s@ 10ppm	143s@ 10ppm	9.3%@ 1ppm	6
$Ti_3C_2T_x$ /SnO_2	0.5-100	0.5	36s@ 50ppm	44s@ 50ppm	-	7
MoS_2@ MoO_3	1-50	1	45s@ 50ppm	53 s@ 50ppm	-	8
$Ti_3C_2T_x/TiO_2$ /MoS_2	10-800	0.5	117s@ 100ppm	88s@ 100ppm	6.31%@ 100ppm	9
PANI/Pt /MoS_2	1-500	0.25	15s@ 50ppm	103s@ 50ppm	16.64%@ 50ppm	10
MoS_2 /graphene	25-500	0.72	80s@ 200ppm	70s@ 200ppm	40%@ 200ppm	11
$Ti_3C_2T_x$ /graphene	10-100	10	-	-	7.2%@ 100ppm	12
PANI /MWCNTs /MoS_2	0.25-20	0.25	32s@ 0.25ppm	36s@ 0.25ppm	-	13
V_2CT_x@MoS_2	0.2-1	0.129	9.82s@ 1ppm	24.22s@ 1ppm	8.71%@ 0.2ppm	This work

Table S2 Comparison of this study with previously reported ammonia sensors in terms of response values

Materials	Response	Year published	Ref.
Ti_3C_2	2%@50ppm	2019	[14]
rGO/ZnO	3.05%@50ppm	2016	[15]
$Ti_3C_2T_x$@TiO_2	3.1%@10ppm	2019	[16]
PANI/rGO	13%@15ppm	2019	[17]
NiWO4/MWCNTs	13.07%@50ppm	2021	[18]
SWCNT/PPY/PA	2.2%@1ppm	2020	[19]
PEDOT:PSS/N-MXene	13%@10ppm	2021	[20]
Ti3C2Tx/PVDF-ZIF-67	4.7%@25ppm	2024	[21]

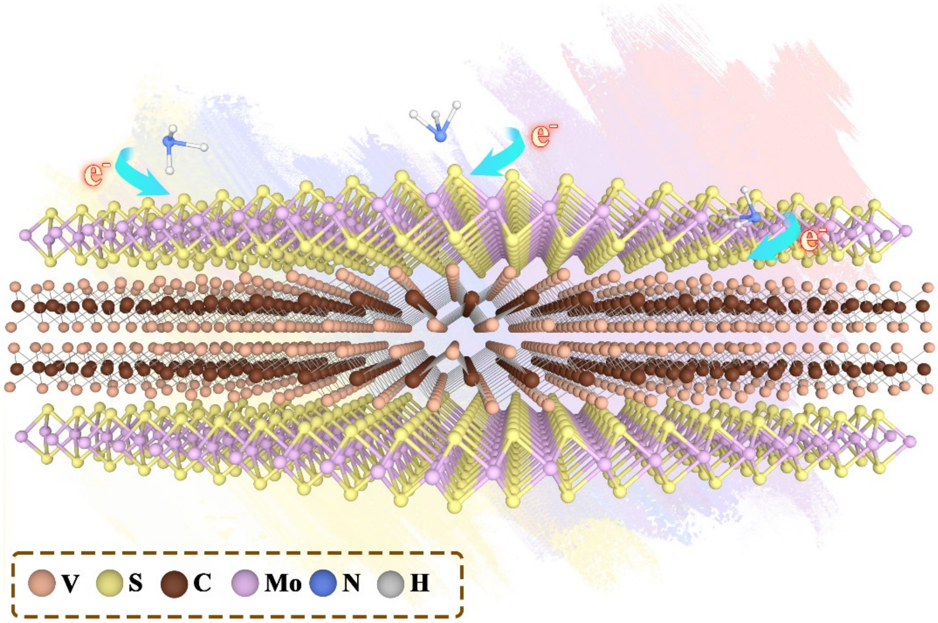

Fig. S16 Gas sensing mechanism toward NH_3 gas for the V_2CT_x@MoS_2 nanohybrid.

References

1. G. Kresse and J. Furthmuller, *Phys Rev B Condens Matter*, 1996, **54**, 11169-11186.
2. J. Hafner, *J Comput Chem*, 2008, **29**, 2044-2078.
3. J. P. Perdew, K. Burke and M. Ernzerhof, *Phys Rev Lett*, 1996, **77**, 3865-3868.
4. G. Kresse and D. Joubert, *Physical Review B*, 1999, **59**, 1758-1775.
5. S. Grimme, J. Antony, S. Ehrlich and H. Krieg, *J Chem Phys*, 2010, **132**, 154104.
6. S. Wang, B. Liu, Z. Duan, Q. Zhao, Y. Zhang, G. Xie, Y. Jiang, S. Li and H. Tai, *Sensors and Actuators B: Chemical*, 2021, **327**,128923.
7. T. He, W. Liu, T. Lv, M. Ma, Z. Liu, A. Vasiliev and X. Li, *Sensors and Actuators B: Chemical*, 2021, **329**,129275.
8. S. Singh, J. Deb, U. Sarkar and S. Sharma, *ACS Sustainable Chemistry & Engineering*, 2021, **9**, 7328-7340.
9. X. Tian, L. Yao, X. Cui, R. Zhao, T. Chen, X. Xiao and Y. Wang, *Journal of Materials Chemistry A*, 2022, **10**, 5505-5519.
10. X. Tian, X. Cui, Y. Xiao, T. Chen, X. Xiao and Y. Wang, *ACS Applied Materials & Interfaces*, 2023, **15**, 9604-9617.
11. A. Jian, J. Wang, H. Lin, S. Xu, D. Han, Z. Yuan and K. Zhuo, *ACS Omega*, 2022, **7**, 11664-11670.
12. S. H. Lee, W. Eom, H. Shin, R. B. Ambade, J. H. Bang, H. W. Kim and T. H. Han, *ACS Applied Materials & Interfaces*, 2020, **12**, 10434-10442.
13. D. Zhang, Z. Wu, P. Li, X. Zong, G. Dong and Y. Zhang, *Sensors and Actuators B: Chemical*, 2018, **258**, 895-905.
14. M. Wu, M. He, Q. Hu, Q. Wu, G. Sun, L. Xie, Z. Zhang, Z. Zhu and A. Zhou, *ACS Sensors*, 2019, **4**, 2763-2770.
15. H. Tai, Z. Yuan, W. Zheng, Z. Ye, C. Liu and X. Du, *Nanoscale Research Letters*, 2016, **11**, 1-8.
16. H. Tai, Z. Duan, Z. He, X. Li, J. Xu, B. Liu and Y. Jiang, *Sensors and Actuators B: Chemical*, 2019, **298**,126874.
17. C.-T. Lee and Y.-S. Wang, *Journal of Alloys and Compounds*, 2019, **789**, 693-696.
18. M. Yang, C. Au, G. Deng, S. Mathur, Q. Huang, X. Luo, G. Xie, H. Tai, Y. Jiang, C. Chen, Z. Cui, X. Liu, C. He, Y. Su and J. Chen, *ACS Applied Materials & Interfaces*, 2021, **13**, 52850-52860.
19. W. Xuan Du, H.-J. Lee, J.-H. Byeon, J.-S. Kim, K.-S. Cho, S. Kang, M. Takada and J.-Y. Kim, *Journal of Materials Chemistry C*, 2020, **8**, 15609-15615.
20. J. Qiu, X. Xia, Z. Hu, S. Zhou, Y. Wang, Y. Wang, R. Zhang, J. Li and Y. Zhou, *Nanotechnology*, 2021, **33**,065501.
21. N. K. Arkoti and K. Pal, ACS Sensors, 2024, DOI: 10.1021/acssensors.3c02551.